Two-photon multifocal microscopy for in vivo single-molecule and single-particle imaging

Vlieg, R.C.

Chapter 1
Introduction

The ability to image single molecules in live cells and organisms, for understanding cellular processes, has opened new possibilities over traditional averaging techniques. Fundamental to the quality of any microscopy experiment in biology is the temporal and spatial resolution. Directly related to resolution are the integration time, duration and at which signal-to-noise ratio these observations can take place. Numerous microscopy techniques have been developed to optimize abovementioned properties.

In this thesis we investigate the ability of two-photon multifocal microscopy for single-molecule microscopy in live cells and organisms. Two-photon excitation combined with multifocal scanning has the potential to achieve, high (temporal) resolution imaging at a low background. These characteristics are indeed beneficial for single-molecule experiments and any live cell imaging assay. However, two photon excitation generally requires high excitation powers, which may limit photon stability and cell integrity.

This chapter introduces the challenges of light microscopy for *in vivo* imaging and explains the main principles behind our used imaging technique. We also compare two-photon multifocal scanning with the increasingly popular microscopy technique of light-sheet microscopy.

1.1 *IN VIVO* MICROSCOPY

By looking at any tissue it becomes apparent that the propagation of light is strongly influenced by it. Also, the lack of contrast in the complex (extra)cellular environment requires highly specific markers to resolve a molecule or structure of interest. For this, a great variety of fluorescent, luminescent and/or scattering labels are available. Here we highlight some of the main physics that describes the boundaries of *in vivo* imaging.

1.1.1 SCATTERING AND ABSORPTION OF LIGHT IN CELL TISSUE

Cells, extracellular structures (collagen fibers, elastin, etc.) and fluids all combine into a complex optical system. Light needs to penetrate the tissue, travel towards the structure of interest and travel back to the objective for optical detection. During this process, light is subject to scattering and absorption, which hinders imaging and impairs image quality. The optical properties of a tissue can be described in terms of its absorption coefficient, μ_a (cm^{-1}), scattering coefficient, μ_s (cm^{-1}) and anisotropy g[1].

μ_s is defined as the probability that light is scattered per unit path length. Optical scattering can occur by particles that have a refractive index different to their surrounding medium, or due to a medium which has a continuous but fluctuating refractive index[2]. As light is scattered when travelling towards the focal spot, or back to the objective to be collected for detection, it loses its spatial coherence. In other words, a focused light beam is transformed to a diffuse bundle, resulting in dim and blurred images.

Mie theory describes the scattering of light from a sphere in a homogenous medium[3]. Scattering depends on particle diameter and the refractive index and wavelength of the incident light. Cell tissue contains a variety of particles and differences in refractive indices, making it much harder to grasp theoretically. Different tissues have different scattering characteristics which also depends on wavelength, see Figure 1.1a[4]. A common approximation for μ_s is given by:

$$\mu_s = \frac{a}{1-g}\left(\frac{\lambda}{500}\right)^{-b} \tag{1.1}$$

where g denotes the anisotropy and a and b are experimentally determined factors which can vary greatly between tissue[5]. Anisotropy g denotes the scattering direction at upon encountering a particle. For g = -1 and g = 1 light is scattered completely in backwards or forward direction, respectively. $g = 0$ indicates that scattering is evenly distributed in all directions. As such, g has a large influence on the scattering characteristics of tissue. In most biological tissues light is

predominantly scattered in a forward direction ($g > 0.9$)[1], resulting in an exponential loss of power with the thickness of the sample.

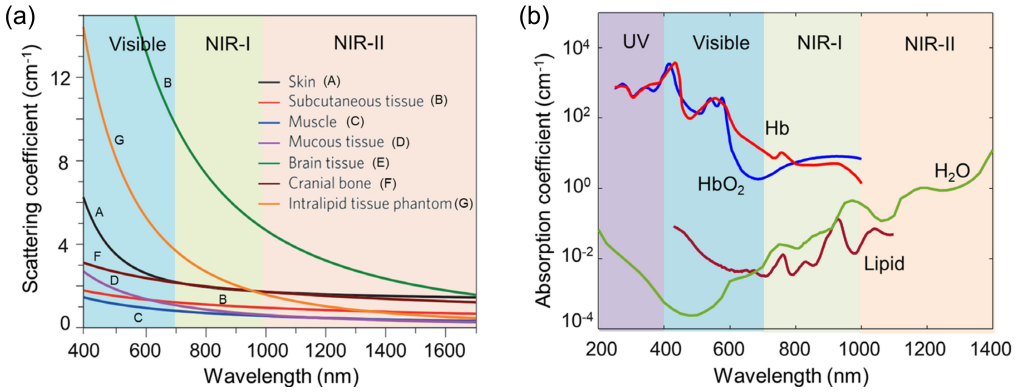

Figure 1.1: The main sources of light attenuation in microscopy are absorption and scattering. (a) The scattering coefficient as a function of wavelength varies in different types of tissue. Scattering decreases exponentially as the wavelength increases. (b) The absorption coefficient of a selection of biological materials as a function of wavelength. Absorption by hemoglobin (Hb) is significantly reduced for NIR wavelengths. In tissue where blood is absent, absorption is dominated by water and lipids. Adapted from [4].

Besides scattering, light can be absorbed by any molecule it encounters, resulting in a similar exponential decay. μ_a is defined as the probability of a photon being absorbed in a medium per unit path length. Similar to scattering, the absorption of light is wavelength dependent, see Figure 1.1b. Pigmented biological tissues feature much higher μ_a and impede high quality imaging.

The combination of scattering and absorption limits the number of photons that contribute to the signal that is collected by the detector. The number of photons (I) of wavelength (λ) at depth (z) inside a medium can be modelled as:

$$I(\lambda) = e^{-z(\mu_a(\lambda)+\mu_s(\lambda))} \tag{1.2}$$

This combination of scattering and absorption limits the imaging depth for most traditional microscopy techniques to ±100 µm. For studying larger organisms like mice, this often means that tissue needs to be removed and imaged *ex vivo*. High absorption can be further mitigated by studying organisms or tissue that lack pigment. Additionally, the μ_a and μ_s can be significantly reduced by optical clearing techniques, which minimize refractive index mismatches or break down highly opaque structures [6–8]. For live imaging such harsh chemical preparation steps cannot be applied. However, recent developments in optical engineering like wavefront shaping, can be used to focus the light in highly turbid media[9]. Circumventing high absorption and scattering all together may also be an option. Small transparent model organisms, like round worms (*Caenorhabditis elegans*)[10] and zebrafish embryos (*Danio rerio*)[11], have for

this reason become popular in microscopy assays. The abovementioned examples form only a limited part of methods that are available on tackling the problems that optical microscopy has with opaque tissues. Dealing with absorption and scattering is therefore, arguably one of the most important challenges in *in vivo* microscopy.

1.1.2 CONTRAST LABELING

Because scattering and absorption impede microscopy imaging, alternative methods to achieve optical contrast are desirable. Self-luminescent structures, for example using fluorescence, relieve this constraint. Most biological structures feature a small amount of autofluorescence. Autofluorescence is the natural emission of light by biological structures as they absorb light, which increases the background signal of the image, see Figure 1.2[12]. So in order to resolve a specific structure of interest it is necessary to tag it with a light-emitting marker. These markers must be bright enough to be resolved in optical dense tissue and above the autofluorescent background. Roughly, contrast markers can be subdivided into three categories: fluorescent proteins, organic dyes and nanoparticles.

Fluorescent proteins (FPs) are widely used in microscopy. By cloning the genetic code of a FP into a gene, a specific protein is fluorescently tagged. Different color FPs are available and their specificity, versatility, convenience and minimal steric and biological interference has made FPs the most popular method for bio-imaging[13]. A drawback of FPs is their relatively small absorption cross section, which reduces the efficiency of excitation. Also, FPs have a limited photo-stability. When excited, they are prone to changes in conformation, oxidation, or react with free radicals in the environment and lose fluorescence, referred to as photobleaching. In long time-lapse measurements, photobleaching limits the duration of the experiment as there is a maximum to the number of times a fluorophore can cycle between the ground and the excited state and emit a photon[14].

Organic dyes offer a larger absorption cross section and quantum efficiency than FPs and span a wide spectral range of excitation wavelength[15]. This makes organic dyes versatile and bright markers. Multiple organic dyes can be attached to a single target, which can increase brightness even further. For this reason, dyes are often applied as markers for single-particle tracking microscopy. Microinjected liposomes for example, have been are tracked inside whole organisms[16].

The labelling of proteins with organic dyes cannot be done directly via genetic encoding. Therefore, one of the main challenges is attaching dye-labels to a specific target biomolecule. Several strategies are available for tagging, like enzyme-catalyzed labeling via post-translational modifications. For example, biotin and biotin acceptor peptides have been used for tagging membrane surface proteins[15]. An increasingly popular strategy is to genetically encode a HaloTag, which is a peptide designed to bind to synthetic ligands. These synthetic ligands can be attached to an organic dye for imaging of targeted proteins[17]. Delivery of organic dyes inside

of the cells can be done via: acetomethoxymethyl (AM)-ester derivatization, microinjection, gene guns, cationic liposomes, cell membrane manipulation and endocytosis [18,19]. Most of these biomolecule tagging strategies are effective on single cell experiments but not for whole organisms. Photobleaching is also still an issue for organic dyes similar to FPs.

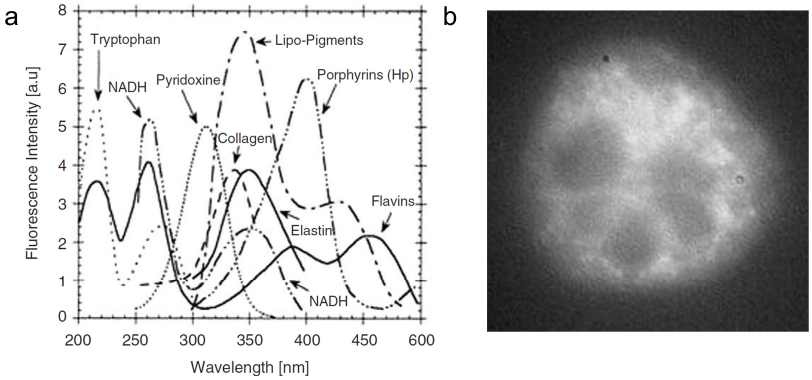

Figure 1.2: **Naturally occurring proteins fluoresce when excited at appropriate wavelengths.** (a) Excitation spectra of a selection of proteins that can be found in nearly every cell. (b) Autofluorescence of a leukocyte when excited at 365 nm. At these wavelengths autofluorescence can impair the SNR of the contrast labels. Adapted from [12].

Nanoparticles such as quantum dots (QDs) are unencumbered by photobleaching. QDs also feature an absorption cross section a factor 4 to 40 higher than fluorescent dyes and exhibit narrow excitation spectra which can extend further into the near-infrared (NIR) wavelengths[20]. These properties make QDs attractive for high-resolution single particle tracking microscopy and can be effectively used with NIR excitation sources[21]. QDs do however, blink, which entails temporary loss of signal for up to tens of seconds. This hampers their use for single particle tracking[22].

Noble metallic nanoparticles, like gold or silver nanospheres or nanorods, do not feature any blinking or bleaching and exhibit even brighter luminescence than QDs[23]. The conducting electrons of a metallic nanoparticle can couple with light, which greatly enhances both the absorption and emission of light. The oscillation frequency of this localized surface plasmon resonance (LSPR) is dependent on the material of the particle, its aspect ratio and the refractive index of the surrounding medium. Gold spherical particles have a LSPR of ±532 nm, elongated gold nanorods (GNRs) have a slower oscillation frequency and the absorption peak is therefore red-shifted, ranging to infrared wavelengths. The excitation spectrum can be tailored to the measurement setup. Moreover, relatively easy surface bio-functionalization makes GNRs compelling contrast markers for high accuracy 3D single particle tracking[24]. The high sensitivity of the LPSR to the surrounding refractive index has been exploited for highly specific detection of single molecules[25]. Similar to organic dyes, transport of QDs and GNRs to their target

biomolecules in live cells or organisms is one of the main challenges. Also the large size (1-50 nm) may induce steric hinder when attached to the smaller target proteins [20].

Comparing the three presented labeling methods, there is a trade-off between brightness, biocompatibility and steric hinder. The brightness of organic dyes and nanoparticles for example, makes them especially useful for single particle tracking in larger or more optical dense tissue but specific labeling in live tissue remains challenging. The simple, highly specific and well established labeling method for FPs make them the main method for fluorescent labeling of biological samples. Therefore, when developing novel microscopy modalities for *in vivo* imaging, special attention should be directed towards compatibility with FPs.

1.1.3 PHOTOTOXICITY

A high photon emission rate is especially necessary for resolving fast cellular processes with a good spatial resolution. The high excitation power that is required is potentially damaging for the sample[26,27]. Phototoxicity can lead to extreme damage like cell death, which is often preceded by morphological changes such as: membrane blebbing, vacuole formation, mitotic arrest and nuclear fragmentation[26,28,29]. However, adverse effects of illumination that are less apparently manifested may still impair the function of the biological system. Less noticeable effects of phototoxicity include: slowdown of cellular growth processes[30], impaired neuronal function[31], and loss of the mitochondrial membrane potential[32]. Awareness of the more subtle phototoxic effects can result in more reliable and reproducible data and is important to consider for any *in vivo* experiment.

Phototoxicity can be caused via different pathways. The presence of reactive oxygen species (ROS) is the most prevalent[33]. A natural variety of organic molecules absorb visible light and subsequently get degraded when they react with oxygen. During this process ROS are produced including superoxide radicals, hydroxyl radicals and hydrogen peroxide[34]. ROS can oxidize DNA, causing mutations, or proteins and unsaturated fatty acids in lipids, rendering them non-functional. ROS have been shown to impede the function of enzymes or change the global state of the cell cytoplasm or mitochondria[35]. Similar to naturally occurring light-absorbing proteins, the excitation of fluorophores can produce ROS[36]. Hence, the location of a fluorophore inside a cell has a large effect on the photosensitivity of that cell[37]. Excited nanoparticles can also create ROS as the energized electron can react to neighboring oxygen molecules[38]. Photobleaching and phototoxicity are closely connected to each other, although they are distinctly different phenomena. An absence of photobleaching is a good indicator of illuminating at a safe level. However, in many live samples FPs are continuously produced and hence make photobleaching an unreliable method for assessing phototoxicity[28].

ROS scavenging mechanisms, like antioxidants, have developed through evolution to remove ROS from cells. Every organism or tissue has, different resistance to phototoxic effects shaped by their living environment[33]. For example, *Drosophila* (fruit fly) and *C. elegans*

(ringworm) appear to be more resistant to laser illumination than zebrafish embryos[39]. However, the additional production of ROS during light exposure can rapidly overwhelm the natural defenses of a biological system. Once this happens the health of an organism quickly deteriorates, see Figure 1.3a/b.

The phototoxicity threshold for an organism or cell can be determined by measuring phototoxic effects at different light doses[40]. The threshold can be moved to higher light intensities by adding ROS scavengers, like antioxidants [41], ascorbic acids[42] and flavonoid rutin[43] to the imaging medium. These methods are more effective for single-cell experiments than for whole organisms due to the endothelial cell barrier that restricts access to the internal cells. To reduce phototoxic effects in larger samples, strategies like temporally pulsed illumination[44,45] or spatially selective illumination (e.g. TIRF[46], two-photon[47] and light-sheet[48] microscopy), have been explored, as well as longer excitation wavelengths and reduced peak powers.

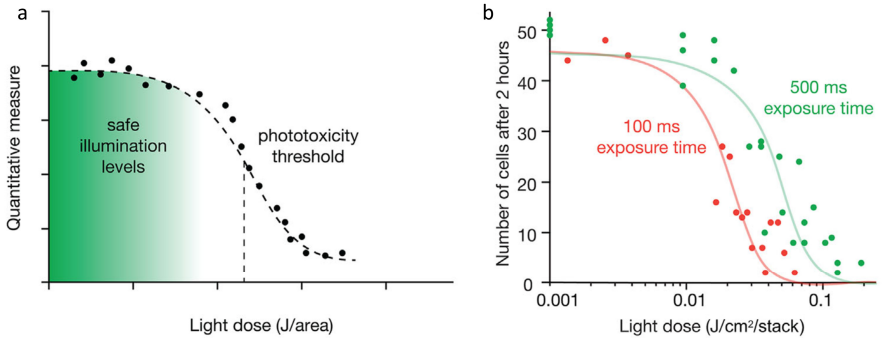

Figure 1.3: High intensity light irradiation can impair cellular mechanisms and lead to cell apoptosis. (a) Typical shape of a phototoxicity curve. When the dose exceeds a threshold, the natural oxygen scavenging defense mechanisms of a cell are overwhelmed and the rate at which cells perish increases drastically. (b) Experimental data on cell death as a function of light dose with two different illumination times. Adapted from [28].

In addition of reactive pathways, absorption of light by tissue can cause local heating and lead to cavitation and heat-induced morphological changes. Absorption scales with laser power. Most microscopy schemes use low enough illumination powers that heating of the sample does not have a major influence on the cellular metabolism. The non-linear excitation methods that we describe in this thesis are more likely to cause heating due to the substantially higher laser power [49,50]. Imaging of transparent and non-pigmented samples should generally prevent most heat-related phototoxic effects by reducing scattering and absorption.

In any *in vivo* imaging application the right balance between sample health, signal-to-noise ratio and spatial and temporal resolution needs to be found, see Figure 1.4. The highest signal to noise results in the best quality images. However, the necessary higher illumination intensity impairs sample health and increases photobleaching. A related factor is the desired temporal resolution. Reducing the acquisition time reduces the amount of signal proportionally. The

spatial resolution of an image is important for resolving the smallest details. Distribution of light over a larger area reduces signal intensity per pixel and can be rescued by longer integration times. Hence, one of these parameters cannot be optimized without compromising the others. Novel developments in optical microscopy are bound by these constraints and the challenge is to find a clever method to push the physical limits set by spatial resolution, temporal resolution, signal-to-noise ration and minimal biological damage.

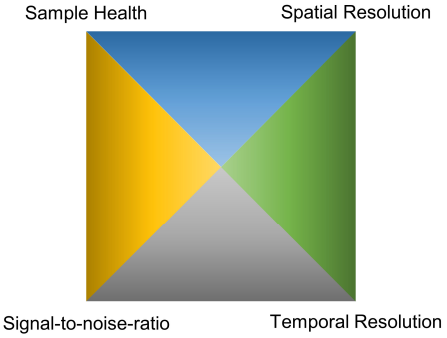

Figure 1.4: **The main condendrum for live imaging.** One parameter cannot be optimized without compromising the others.

1.2 MICROSCOPY TECHNIQUES

Wide-field epi-illumination is arguably fluorescence microscopy in its most simplistic form. A collimated excitation beam homogeneously illuminates the sample at a straight angle (i.e. epi-fluorescence) and the whole field-of-view (FOV) is illuminated in a single instance. Images are acquired rapidly by a CCD or sCMOS camera. Although wide field illumination is straightforward and high temporal resolutions are easily realized, out-of-focus fluorescence contributes to a large background signal and limits observations to two dimensions.

The background signal is greatly suppressed by implementing techniques which reduce the illumination volume such as total internal reflection fluorescence (TIRF) microscopy[51] and highly inclined and laminated optical sheet (HILO) microscopy[52]. In practice, the reduction in excitation volume limits these techniques to smaller samples and imaging is also limited in two dimensions (2D). By introducing a rasterized illumination pattern, referred to as structured illumination microscopy (SIM), background can also be computationally eliminated[53]. SIM effectively separates signal inside the focal plane from outside the focal-plane and allows to computationally dissect a sample in three-dimensions (3D)[54].

Another way of reducing background signal and improve 3D sectioning is to focus the laser beam into a single point and collect signal from this focal volume that is confined in 3D.

In laser scanning confocal microscopy (LSCM) out-of-focus fluorescence is spatially blocked by a pin-hole positioned in the emission path, an image is then reconstructed for serial measurements in which the focus is raster scanned through the sample. The sample is thus optically sectioned into thin slices and signal is collected with a low-noise, high sensitivity photomultiplier tube or photo-avalanche diode. The focused laser beam in combination with the pinhole enables deeper imaging than epi-fluorescence illumination at lower illumination power[28]. The ability to image a sample in 3D with relative ease has made LSCM a standard for live microscopy imaging. However, the serial acquisition impedes temporal resolution and life cell imaging is limited to slow processes. Despite that the light is focused, in-focus and out-of-focus fluorophores are still being bleached which limits the duration of the measurement.

1.3 TWO-PHOTON MICROSCOPY

In this thesis we use two-photon excitation (TPE) to mitigate some of the challenges *in vivo* environments impose on light microscopy. One of the ultimate goals is to reach single molecule sensitivity, which is the basis for the recent super-resolution revolution, that has boosted the performance of modern microscopy techniques. Though the combination of TPE and single molecule imaging has so far been heavily limited by photobleaching, the development of ultra-sensitive scientific CMOS cameras, in combination with advanced structural illumination schemes and better control over NIR lasers warrants a fresh effort in this direction.

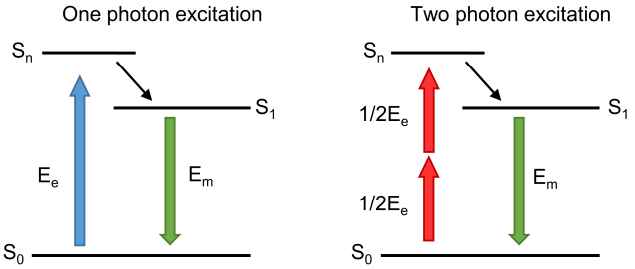

Figure 1.5: **Jablonski diagram for the excitation of a fluorophore using one photon and two photon excitation.** Half the energy per excitation photon is necessary for 2 photon excitation, which extends the excitation wavelengths to NIR. Once excited, the relaxation of the fluorophore follows the same pathway.

Invented in 1990, two-photon microscopy (TPM) is based on the excitation of a chromophore with two-photons instead of the more conventional one-photon excitation (OPE), see an illustration in Figure 1.5. Conventional OPE techniques use excitation light in the UV or visible light range to excite the chromophores of interest. For TPE, the use of two-photons

means that roughly half the energy per photon is required to excite a molecule, extending the excitation source to near-infrared (NIR) wavelengths. The absorption of two photons needs to occur within the relaxation time of a fluorophore (10^{-9} sec) which means that TPE is only effective at very high light intensities[55]. To achieve this, TPE is implemented using a focused beam in combination with femtosecond pulsed lasers[56]. Pulsed laser sources generate high peak intensities (kW-GW) necessary for TPE, while the average laser power remains relatively low (2-5 W), reducing linear absorption and thus heating and phototoxic damage to the sample. For a more quantitative understanding of the parameters involved for TPE, the probability (p) of two-photon absorption per laser pulse can be described as[57]:

$$p = \frac{P^2 \delta}{\tau_p f_p^2} \left(\frac{NA^2}{2hc\lambda} \right)^2 \tag{1.3}$$

with P the average laser intensity (W cm^{-2}), δ the two-photon absorption cross section of the chromophore (typically 10^{-50} cm^4 s) at the excitation wavelength λ (typically 650 – 1300 nm), τ_p the pulse width (typically 80 – 200 fs), f_p the repletion rate (typically 60 – 160 MHz), NA the numerical aperture, h Planck's constant, and c the speed of light. The quadratic dependence of signal to laser power characterizes TPE as a non-linear excitation mechanism. From equation 1.3 it is clear that not only the light intensity affects p, but also the chosen objective, as p scales with NA^4. With a higher NA the focal volume is decreased, concentrating the light more efficiently. After saturation of the fluorophore is reached (p=1), the signal is limited by the repetition rate of the laser. However, previous reports show that photobleaching is severe at these excitation powers and drastically impair measurement times[58].

Most TPMs use femtosecond pulsed laser sources, benefiting from the increase in p as a result of shorter pulse width, combined with the relative wide availability of Ti:Sa lasers. A typical Ti:Sa laser can produce 100 fs pulses at a rate of around 80 MHz with a tuning range between 700-1000 nm. However, TPM has also been done with picosecond and continuous wave (CW) lasers[59,60]. A CW laser necessitated around 200 times the average laser power compared to a standard Ti:Sa laser to achieve similar signal, illustrating the advantage of using pulsed lasers to reduce average laser power. The real advantage of using CW lasers is to reduce system costs as diode CW IR lasers with sufficient power are available for <€1000, whereas a typical Ti:Sa laser costs €100k>.

A major advantage of TPE is that biological tissue features less scattering and absorption at NIR than visible wavelengths. This so-called NIR-window, as plotted in Figure 1.1, makes TPM a powerful technique for deep-tissue imaging. Typically, TPM extends imaging depth in rodent brains from ±100 µm in confocal OPE to ±500 µm[5]. The deeper imaging depth has made TPM able to perform live imaging of transient neuronal Ca^{2+} fluxes in rodent brains, where one-photon excitation (OPE) failed[61]. Another interesting application for TPM is fluorescent correlation spectroscopy (FCS). FCS is based on the autocorrelation of the diffusion of a small

number of molecules through the focus. Inside live cells TPE made it possible to do FCS, where background signal would be too high for OPE to resolve single fluorophores[62].

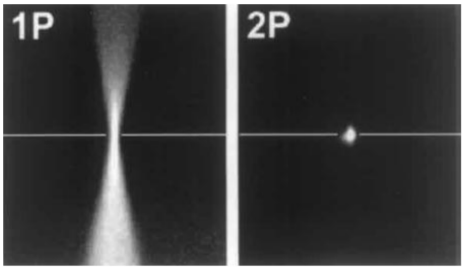

Figure 1.6: With one-photon excitation fluorophores outside the focal volume are excited. In contrast, the low probability of two-photon excitation confines fluorescence to the focal volume of the objective. Adapted from [56].

The intrinsic optical sectioning of TPE means that background fluorescence is eliminated without the need for a pin-hole, see Figure 1.6. Background is further reduced by the exceptionally large anti-Stokes spectral difference between excitation and emission photons, facilitating spectral separation of the two.

There are many theoretical methods on how to estimate the resolution of a microscope. A relatively straightforward and common approach is by calculating the full width at half maximum (FWHM) of the PSF according to Rayleigh's criterion. For LSCM, the lateral ($\omega_{r,OP}$) and axial ($\omega_{z,TP}$) resolution based on Rayleigh's criterion is[64]:

$$\omega_{r,OP} = \frac{0.51\lambda}{NA} \tag{1.4}$$

$$\omega_{z,OP} = \frac{0.88\,\lambda}{(n - \sqrt{n^2 - NA^2}} \tag{1.5}$$

with *n* the refractive index of the medium. Please note that equation 1.4 and 1.5 slightly deviate from the standard Rayleighs' criterion of $\omega_{r,OP} = 0.61\lambda/NA$ and $\omega_{z,OP} = 2\lambda n/NA^2$ due to the inclusion of the pin-hole aperture.

For a standard TPM the resolution of the microscope is purely defined by the size of the point spread function[65]. As TPE roughly uses twice the wavelength to excite the same fluorophore as OPE the resolution intuitively should be worse. However, the quadratic dependence of signal on laser power confines the excitation to a narrower volume. An estimation of the resolution of TPM could be the square root of equations 1.4 and 1.5. A more common definition however, is by the numerical estimation for $\omega_{r,TP}$ and $\omega_{z,TP}$ based on fitting quadratic

Gaussians to the intensity distribution model of Richards and Wolf, which results in a slightly different values:[63]

$$\omega_{r,TP} = \frac{0.541\lambda}{\sqrt{2}NA^{0.91}} \tag{1.5}$$

$$\omega_{z,TP} = \frac{1}{\sqrt{2}}\left(\frac{0.886\lambda}{n - \sqrt{n^2 - NA^2}}\right) \tag{1.6}$$

assuming NA > 0.7 and the detector meets the Nyquist criteria. Equations 1.5 and 1.6 do not take any side-lobes of the Airy rings into account, which will be negligible for a standard TPM. However, when the excited fluorophore approaches saturation (p = 1), the main lobe would flatten and the side lobes become more prominent. When this happens the optical resolution of a TPM starts to deviate from equation 1.5 and 1.6. For super-resolution, the localization accuracy can be determined by accounting for shot-noise, which reduces the uncertainty in positioning by $\sqrt{N}$, with N photons. Therefore, brighter fluorophores and thus higher excitation intensities are desirable. For normal biological imaging however, the photon flux necessary to reach fluorophore saturation would result in high photobleaching and phototoxicity, impairing sample integrity. In practice, saturation effects are only relevant for highly efficient two-photon labels, such as QDs and metallic nanoparticles[66,67].

The difference in resolution between linear and non-linear excitation can be compared using equations 1.4-1.6. For example, exciting a fluorophore at 400 nm with an NA=1.1 yields $\omega_{r,OP}$ = 0.19 µm and $\omega_{z,OP}$ = 0.60 µm. For exciting the same fluorophore with TPE at 800 nm results in $\omega_{r,TP}$ = 0.28 µm and $\omega_{z,TP}$ = 0.86 µm. As such, the theoretical resolution of a TPM is only moderately worse compared to a confocal microscope. However, in practice the higher scatter coefficient of visible light inside tissue and the lower background fluorescence of TPM generally results in resolution similar or better than that of a LSCM, especially at larger imaging depths[68]. Therefore, the consensus is that confocal and TPM have similar image resolution which shifts in favor of TPM at larger imaging depths.

Photobleaching and phototoxicity with TPE is more elusive and less well understood than with OPE. Fluorophores outside the focal volume are not excited, which confines the phototoxicity and photobleaching. Inside the focal volume however, the large flux of photons can promote already excited fluorophores to higher energy states, which increases their reactivity with surrounding molecules. This results in faster bleaching inside the focus than with OPE [69–72] and therefore makes TPM more beneficial for the imaging large volumes of bigger samples where more fluorophores are available. The two-photon photobleaching rate (τ) scales with laser power (P) as:

$$\tau = A * P^c \quad (1.7)$$

empirically, with amplitude *A* and exponent *C*. Values for *C* between 2.1 – 5.1 have been dependent on: type of fluorophore[58,73], laser pulse width [74,75], laser repetition rate[76] and surrounding temperature[58]. Using low NA objectives for illumination has also shown a strong decrease in photobleaching, suggesting that reduced peak intensities have a significant role in bleach rates[77]. The >2 exponential dependence indicates a sensitive relationship between bleach rate and excitation power. Thus reduction of the laser power should be paramount in any TPM measurement in order to keep phototoxicity minimal.

1.3.2 MULTIFOCAL SCANNING

Abovementioned advantages have made TPM an excellent technique for the imaging of large volumes in opaque larger organisms. However, the temporal resolution of faster scanning the laser in a serial fashion remains limited. The more so, because most commonly used fluorophores feature a poor two-photon absorption cross section which requires extended integration times[78]. Increasing laser power offers a limited solution due to the exponential dependence of bleach rate and phototoxicity (eq. 1.7). Conventional TPM does not have sufficient temporal resolution for imaging fast cellular processes or to capture single particles or molecules traveling inside living organisms.

Higher framerates can be achieved while keeping phototoxicity low by splitting the laser beam into multiple beamlets. By multiplexing the excitation volume and increasing the total laser power proportionally, the peak power per focus remains unchanged. Collection of the signal from the multiple foci requires array detectors such as sCMOS or EM-CCD cameras. The use of wide-field detectors means that the lateral resolution differs from a conventional TPM, defined by equation 1.5. The lateral resolution is now simply defined by the emission light and thus can be expressed by the standard Rayleigh criterion of $0.61\lambda/NA$, which would not discriminate between OPE and TPE.

Two-photon multifocal microscopy (TPMM) has been done with microlens arrays (MA), microlens discs[79], cascade beam splitters[80], spatial light modulators (SLM) or diffractive optical elements (DOE). Setups using MAs, beam splitters or DOEs split the laser beam in multiple beamlets, after which they are scanned by scanning mirrors. SLMs on the other hand do not require any mechanical scanning; by applying a computer generated hologram, any arbitrary number of foci, their position and intensity can be defined accordingly[81]. Previous studies show a significant increase in imaging speed with TPMM compared to single point scanning. For example, using a SLM creating an 8 x 8 array of foci, fluorescence lifetime of fluorophores in cells was imaged 64 times faster compared to single-point imaging[82]. The imaging of Ca^{2+} transients in neurons can be extended from one to tens of neurons by positioning the foci to

different points-of-interest using a SLIM[83]. An example of multiplexed monitoring of neurons in mouse brain is depicted in Figure 1.7.

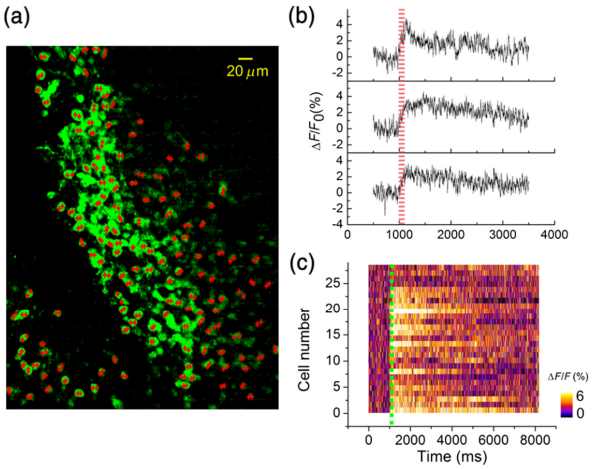

Figure 1.7: **Multiplexing the laser beam allows to measure Ca^{2+} transients in multiple neurons simultaneously at high temporal resolution. (**a) Image of stained neuron cells inside a mouse brain. The red dots annotate the locations of the foci. (b) Three selected time traces showing different kinetics upon stimulation (red dashed line). (c) All 27 time traces of neuron cells which responded to a stimulus. Adopted from [83].

1.3.3 EXPERIMENTAL SETUP

In this thesis we use a TPMM based on a DOE for rapid scanning of the focal plane and a schematic of the setup is shown in Figure 2.1. Per Chapter the details of the used configuration of the setup are described. In short, the DOE diffracts the light into 25 x 25 beamlets oriented in a hexagonal structure. The zeroth-order of the diffraction pattern is blocked by a droplet of soldering tin deposited on a glass slide. The first-order diffraction pattern is collected by a lens and further transmitted to a fast-scanning mirror which spiral-scans the array of foci across the focal plane. For most of the experiments we scanned the array of foci in an Archimedean spiral based on previous work by Van den Broek, et al[24], see Figure 1.8, which can be described in spatial coordinates x and y at time t by:

$$x = A\tau \sin(2\pi n\tau) \tag{1.8}$$

$$y = A\tau \cos(2\pi n\tau) \tag{1.9}$$

$$\tau = \sqrt{\frac{t}{T}\exp\left(\frac{(t/T)^2}{2\sigma^2}\right)} \tag{1.10}$$

with A the amplitude of the spiral, n the number of spirals, T the total exposure time of the camera and σ the width of the Gaussian profile that results from the scanning. Archimedean spiral scanning results in a homogeneous distribution of the light intensity during a single camera exposure, see Figure 1.8. The resulting smooth Gaussian curve minimizes variations in illumination, which is important for a homogeneous illumination of the sample.

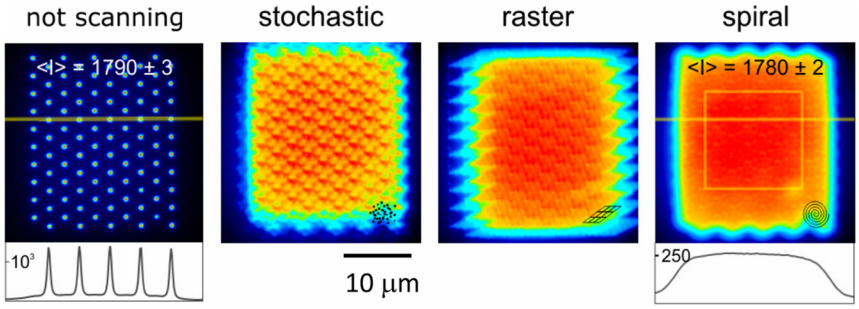

Figure 1.8: **Scanning a grid of foci following an Archimedean spiral generates a homogenous field for wide field two-photon microscopy.** This is the standard method of illumination in this thesis. Adopted from [24].

1.4 LIGHT SHEET MICROSCOPY

Arguably, one of the more recent and exciting microscopy techniques is light-sheet microscopy (LSM). Similar to TPMM, LSM improves image acquisition rates and photobleaching over single-point scanning microscopy. To help understand the advantages and disadvantages of both methods we compare LSM and TPMM. As this thesis is generally focused on TPM, we explicitly discuss two-photon light-sheet microscopy (TPLSM), which due to the non-linear excitation boasts different light-sheet characteristics as compared to single-photon LSM.

In conventional LSM the illumination beam is formed as a static sheet of light, commonly referred to as selective plane illumination microscopy (SPIM)[84]. SPIM utilizes a sheet of light to selectively optically dissect the sample. The light sheet is created by using a cylindrical lens in front of the objective. A second objective is positioned orthogonally to the axis of the illumination objective to collect the signal originating from the light-sheet, see Figure 1.9b. By uncoupling the illumination and the excitation paths, SPIM can rapidly optically dissect a sample with a large field-of-view (FOV), and preventing out-of-focus illumination. The selective illumination not only limits background, it also reduces photobleaching outside the sample and therefore limits the overall phototoxic effects normally associated with OPE methods.

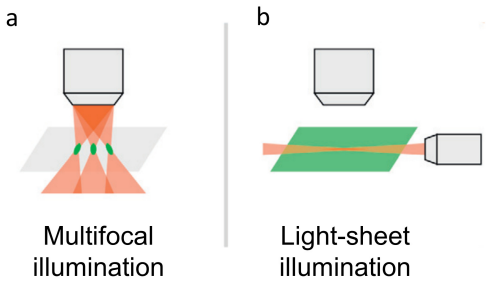

Figure 1.9: **Both multifocal scanning and illumination by a sheet of light allows for deep, fast and gentle optical dissection. (**a) Standard configuration of a multifocal scanning two-photon microscope. Multiple beamlets are focused to increase imaging speed. Illumination and detection are done with the same objective. (b) Standard configuration of a light-sheet microscope. One objective weakly focusses a laser beam to generate a sheet of light. A second orthogonally placed objective collects the fluorescence originating from excited fluorophores. Adopted from [91].

Still, the sheet of light is subject to scattering and broadening when imaging inside tissue. Two-photon SPIM was introduced in 2010 to improve upon SPIM[85–87]. The NIR light is less prone to scattering and allows for deeper imaging depth and less linear absorption[88]. Also, due to the non-linear excitation, scattered illumination photons are less likely to excite out-of-focus molecules which greatly reduces background. However, excitation efficiency decreases drastically in two-photon SPIM compared to single-point TPM due to the quadratic dependence of excitation with laser power. For more efficient two-photon LSM, the cylindrical lens is replaced by a traditional circular one and the illumination beam is focused near the back-focal plane of the objective. By doing so a Gaussian-shaped beam is created which significantly increases light intensity in the excitation volume. Subsequently, the FOV has to be sampled by scanning the illumination beam across the detection focal plane – commonly referred to as two-photon scanned light sheet microscopy (TPSLM). Despite the necessity to scan the sample, TPSLM still results in higher framerates frame rates due a 100-fold increase in signal rate (signal count per unit of average excitation power) compared to two-photon SPIM[77]. The penetration depth of TPSLM can be further improved by a factor of 6 up to 12 when using a Bessel-shaped illumination beam[87,89].

1.4.2 Resolution

In TPSLM, the lateral and axial resolution are decoupled from one another. The lateral resolution is determined by the detection optics, similar to non-SPIM, whereas the axial resolution is determined by a combination of the detection optics and the thickness of the light-sheet itself, see Figure 1.10a. With a thicker light-sheet, SPIM would approach wide-field illumination and lose its ability to optical dissect a sample as out-of-focus fluorescence would become dominant. Hence, reducing the waist of the beam profile is advantageous to increase

SNR and axial resolution. However, to achieve a slimmer waist, a higher focus angle (NA) is necessary which decreases the penetration depth of the beam. Referring to Figure 1.10a, the radius of a Gaussian shaped beam at its thinnest point (ω_0) is described by[90]:

$$\omega_0 = \frac{\lambda}{\pi\, NA} \tag{1.11}$$

The axial resolution as the FWHM of the beam profile ($\omega_{z,LS}$) is then defined as:

$$\omega_{z,LS} = \omega_0 \sqrt{\ln 2} \tag{1.12}$$

The FOV of a DSLM is determined by the propagation of the illumination beam (l_{LS}) while maintaining a certain thickness. Setting the thickness threshold at $\sqrt{2}\,\omega_0$ yields a l_{LS} of[77]:

$$l_{ls} = \frac{2n\lambda}{\pi\, NA^2} \tag{1.13}$$

From these equations the sensitive relationship between the FOV and the axial resolution can be better appreciated. For example, exciting a sample at 800 nm using a NA = 0.1 objective gives ω_{LS} = 2.12 µm and l_{ls} = 67.7 µm. Increasing the NA to 0.2 results in a higher resolution of ω_{LS} = 1.06 µm at a significantly reduced l_{ls} = 16.9 µm. Interestingly, considering an illumination NA of 0.1, TPMM would need a NA of 0.83 (equation 1.6) for the same axial resolution as TPSLM. For higher axial resolution however the FOV would reduce drastically, impairing the imaging of larger samples, see Figure 1.10b/c. Therefore, the illumination NA has to remain low which results in a relative poor axial resolution. See Figure 1.10b/c for a comparison between both imaging modalities in terms of axial resolution and FOV.

TPMM can use much higher NA objectives for both illumination and detection. As such, the excitation volume can stay more confined than TPSLM and would therefore have higher axial resolution and SNR. However, axial resolution inside scattering tissue is not as trivial to define, especially at larger depths. The higher angle at which light enters the sample could result in more scattering events as the path-length through tissue is longer compared to lower NA illumination. Imaging in larger samples like zebrafish embryos (*Danio rerio*), indicated that the lower incident angle of the illumination beam of a TPSLM retained its resolution at deeper imaging depths better compared to single-focus TPM[77]. TPMM would use similar NA as TP-SM and therefore would likely be suffering from similar aberrations in its PSF.

The lateral resolution is solely determined by the NA of the detection objective which is not constrained in NA, in contrast to the illumination objective. Hence, the lateral resolution of LSM should be comparable to TPMM and any other microscope which utilizes a wide-field detector.

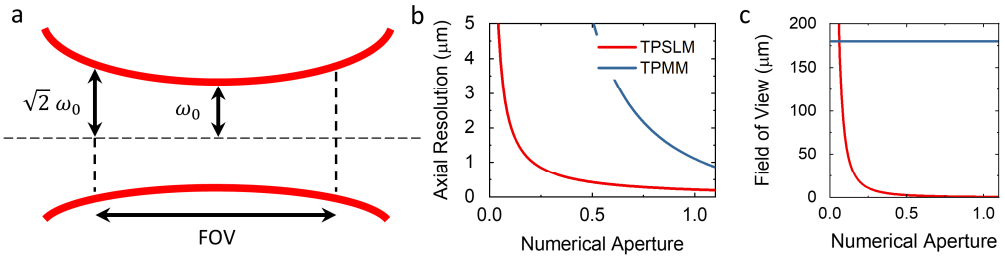

Figure 1.10: The strong correlation between axial resolution and field-of-view limits the axial resolution in two-photon light-sheet microscopy. (a) Schematic of some parameters which dictate the field-of-view and the axial resolution in a TPLSM. (b) Comparison between the axial resolution of TPLSM and TPMM. TPSLM allows to reach the same axial resolutions with lower NA as TPMM. (c) For a useful field-of-view the numerical aperture is generally NA<0.2. Hence also limiting axial resolution. The field-of-view in TPMM is dependent on the emission path optics and detector size, hence more elusive to define. Here we use the width of the excitation plane of our microscope in combination with a 25X NA=1.1 objective.

1.4.3 Phototoxicity

LSM is often referred to as a gentle way of illuminating a sample. Why LSM is considered more gentle than point scanning microscopes originates from the way the incident light of the illumination beam is being used all the way as it travels through the sample. Intuitively, the difference between TPMM and TPSLM in terms of average laser power can be understood as follows. TPMM focusses the light beam after which is disperses again and does not generate signal. In TPSLM the light being send into the sample can continuously excite fluorophores and generate signal, as long as the excitation light is intense enough. For a N times increase in acquisition rate, TPMM would need N^2 more average power, whereas a TPSLM would need $\sqrt{N}$ more power[91]. Therefore, the average excitation power to achieve the same amount of fluorescence in TPSLM is lower. Moreover the lower illumination NA reduces peak intensities which is believed to reduce higher-order bleaching effects[92]. A more thorough explanation on how TPSLM achieves higher signal-rates at similar excitation power can be found in the discussion of Chapter 4 of this thesis.

1.4.4 Complexity and sample mounting

TPMM provides potentially higher resolution, while TPSLM allows for more gentle, deeper and faster imaging. Arguably, the major challenge of TPSLM lies in the complexity of the setup and the elaborate sample mounting procedures. With only few commercial systems available for one-photon SPIM systems, a TPSLM has to be built in-house[93]. TPMM has not been commercialized yet, and therefore it would also be necessary to it from separate components.

The excitation path of a TPMM however, is quite similar to that of a conventional TPM. Multiple beamlets can be generated by placing either a micro lens array or DOE in laser beam after which a scanning mirror scans the beamlets across the focal plane. The transformation from a TP-SM to a TPMM would be roughly complete by replacing the detector (i.e. photomultiplier tube) by a camera. For TPSLM, the orthogonal orientation of multiple objectives makes it structurally more complex. Also, sample mounting is constrained as samples have to be placed in agarose capillaries to be properly aligned with the objectives[94]. Designs are available where conventional sample mounting is possible by making use of AFM cantilevers[95], or highly inclined illumination [96,97], however, this does make the microscope itself more complex or limits the imaging to smaller samples.

At the cost of more complexity, both microscope modalities can be improved in terms of: resolution, imaging depth, image speed and image quality. For example, multiple illumination objectives can be placed opposite of each other for a larger FOV in TPSLM[77,98]. In TPMM, most of the advances can be made by reducing the blurring effect of diffuse emission photons hitting wrong pixels and thereby reducing SNR. This can be done by the likes of operating the microscope in a de-scanned configuration[80,99], pin-hole rejection[100,101] or structured illumination[102,103].

Eventually, the choice between TPMM and TPSLM should be made based on the type of measurements one wants to conduct. If the advantages of TPSLM over TPMM do not add significant information, the extra costs and complexity would likely not justify the investment.

1.5 THESIS OVERVIEW

In this thesis we explore the capabilities of a multifocal two-photon microscope for *in vitro* and *in vivo* experiments down to the smallest scale of single molecules.

We start by exploring the spectroscopy capabilities of the setup in **Chapter 2** for the detection of single molecules using GNRs. The automatic tuning of the laser allowed us to measure the two-photon absorption spectra of GNRs. The quadratic dependence of signal on excitation power yields narrow SPR-bands, which could be used for highly sensitive single-molecule bio-sensing applications. We verified the ability of the setup to resolve single GNRs via: correlation with electron microscope images, light polarization and spectroscopy. The two-photon absorption spectra indeed feature narrower peaks compared to linear contrast methods. By lowering the laser power, GNRs were imaged for extended periods of time without noticeable reshaping, which in general is a major issue for illumination of metallic nanoparticles with high intensity femto pulsed lasers. By changing the refractive index of the media we observed a shift in the LSPR, confirming that spectral measurements can be used for sensing applications. We initiated measurements for single-molecule sensing but stability issues hampered the detection of binding of single molecules to GNRs by two-photon spectroscopy.

In **Chapter 3** we evaluate the performance of the setup for *in vivo* applications and focus on the imaging of single particles. Multifocal scanning allowed for rapid imaging, while the TPE confined excitation to a thin section of the sample. These properties could be valuable for many studies which need high temporal resolution with high SNR. We used GNRs for determining the PSF of the setup. GNRs were also micro injected in zebrafish embryos and tracked as they travelled inside the bloodstream of the embryos. We noticed during measurements in zebrafish embryos that the signal originating from FP expressing endothelial cells was not noticeably reduced by loss in fluorescence due to photobleaching. This led to measuring embryos expressing different FPs and confirmed negligible photobleaching. Pollen embryos were imaged to measure expression of a particular growth factor (LEC1). TPMM revealed highly localized expression of LEC1 which was not observed by one-photon confocal microscopy. Finally, we introduced multi-color imaging for nanometric localization of liposomes in respect to the blood vessel wall in the brain of zebrafish embryos. The combination of low photobleaching, high contrast, high (temporal) resolution, and also in combination with multi-color imaging makes TPMM a very interesting method for high-speed *in vivo* imaging.

Chapter 4 focusses on imaging down to the level of single FPs. The lack of photobleaching and low background of TPMM would make it a promising imaging method for single molecules in live tissue. Two-photon single molecule studies reported however significantly higher bleaching rates compared to single-photon excitation. We did not observe major photobleaching in Chapter 3, which suggests that TPMM provides sufficient fluorescent longevity for single molecule imaging. We validated the ability to measure single FPs *in vitro*

by observing discrete bleaching steps in the acquired time traces and the average measured bleaching times were sufficient for single molecule tracking.

Still, one of the key issues with wide-field detection is blurring of the image by scattered emission photons. Suppressing this phenomenon would allow for higher SNR and provide an opportunity to lower excitation power for even longer bleaching times and less background signal. We subsequently used structured illumination to suppress scatted photons, which indeed worked to increase contrast when imaging inside zebrafish embryos. However, simulations and experiments indicated that structured illumination introduces additional camera read-noise which comes from the necessity to acquire multiple images. We consequently improved the structured illumination method which resulted in superior images compared to spiral illumination.

Finally, we measured single eGFP molecules *in vivo* for extended periods of time. These results showed the novelty of TPMM as a live single molecule tracking technique, and how it provides the opportunity to study cellular processes at very long time scales.

In **Chapter 5 and 6** we highlight two studies which used our setup for measuring single particles in live zebrafish embryos. Zebrafish embryos are widely used model organisms due to their small size, transparency and easy cultivation while still being vertebrates. This makes them popular among toxicology and pathology studies. One study looked into the toxic effects when fish were exposed to, or injected with, metallic nanoparticles. We established in previous chapters that the TPMM is capable of imaging GNRs at high SNR. Combined with the high temporal resolution we could image injected GNRs as they were travelling inside embryo. We managed to image macrophages taking up GNRs, which strengthened the hypotheses that GNRs are not inert and that the immune system does respond to GNRs. The second study investigated the distribution of liposomes which switch their surface charge to negative as they are illuminated by ultraviolet (UV) light. These liposomes have the potential to improve the efficiency and specificity of drug carriers. Negatively charged particles were shown to stick to surrounding endothelial cells and were subsequently endocytosed. An UV diode was placed above the mounted embryo and UV illumination was timed with the two-photon imaging to induce charge reversal. This allowed us to monitor the transition from free flowing to immobile liposomes in real-time. We quantified information on the transition speed from neutral to cationic particles, which is normally obscured in confocal microscopy techniques.

Overall, we enhanced the capabilities of TPM, leading to improved spectral imaging, fast light-sheet imaging, multi-color *in vivo* imaging and single particle and -molecule TPM. The shown biological applications demonstrate that despite physical boundaries there is ample opportunity to improve optical microscopy and explore new applications in biology.

1.6 BIBLIOGRAPHY

1. Jacques, S. L. Optical properties of biological tissues: A review. *Phys. Med. Biol.* **58**, (2013).
2. Jacques, S. L. & Pogue, B. W. Tutorial on diffuse light transport. *J. Biomed. Opt.* **13**, 041302 (2008).
3. Hergert, W. & Wriedt, T. The Mie Theory. *Mie Theory Basics Appl.* 53–71 (2012). doi:10.1007/978-3-642-28738-1
4. Upputuri, P. K. & Pramanik, M. Photoacoustic imaging in the second near-infrared window: a review. *J. Biomed. Opt.* **24**, 1 (2019).
5. Miller, D. R., Jarrett, J. W., Hassan, A. M. & Dunn, A. K. Deep tissue imaging with multiphoton fluorescence microscopy. *Curr. Opin. Biomed. Eng.* **4**, 32–39 (2017).
6. Musielak, T. J., Slane, D., Liebig, C. & Bayer, M. A versatile optical clearing protocol for deep tissue imaging of fluorescent proteins in Arabidopsis thaliana. *PLoS One* **11**, 1–17 (2016).
7. Kurihara, D., Mizuta, Y., Sato, Y. & Higashiyama, T. ClearSee: A rapid optical clearing reagent for whole-plant fluorescence imaging. *Dev.* **142**, 4168–4179 (2015).
8. Warner, C. A. *et al.* An optical clearing technique for plant tissues allowing deep imaging and compatible with fluorescence microscopy. *Plant Physiol.* **166**, 1684–1687 (2014).
9. Vellekoop, I. M. & Mosk, A. P. Focusing coherent light through opaque strongly scattering media. *Opt. Lett.* **32**, 2309 (2007).
10. Corsi, A. K., Wightman, B. & Chalfie, M. A transparent window into biology: A primer on Caenorhabditis elegans. *Genetics* **200**, 387–407 (2015).
11. Kaufmann, A., Mickoleit, M., Weber, M. & Huisken, J. Multilayer mounting enables long-term imaging of zebrafish development in a light sheet microscope. *Dev.* **139**, 3242–3247 (2012).
12. Monici, M. Cell and tissue autofluorescence research and diagnostic applications. *Biotechnol. Annu. Rev.* **11**, 227–256 (2005).
13. Piyaraj, P. The Green Fluorescent Protein (GFP). *Bangkok Med. J.* **05**, 101–102 (2013).
14. Lippincott-Schwartz, J., Altan-Bonnet, N. & Patterson, G. H. Photobleaching and photoactivation: Following protein dynamics in living cells. *Nat. Rev. Mol. Cell Biol.* **4**, (2003).
15. Sameiro, M. & Gonçalves, T. Fluorescent labeling of biomolecules with organic probes. *Chem. Rev.* **109**, 190–212 (2009).
16. Manzo, C. & Garcia-Parajo, M. F. A review of progress in single particle tracking: From methods to biophysical insights. *Reports Prog. Phys.* **78**, (2015).
17. Los, G. V. *et al.* HaloTag: A novel protein labeling technology for cell imaging and protein analysis. *ACS Chem. Biol.* **3**, 373–382 (2008).
18. Torchilin, V. P. *et al.* Cell transfection in vitro and in vivo with nontoxic TAT peptide-liposome-DNA complexes. *Proc. Natl. Acad. Sci. U. S. A.* **100**, 1972–1977 (2003).
19. Waggoner, A. Fluorescent labels for proteomics and genomics. *Curr. Opin. Chem. Biol.* **10**, 62–66 (2006).
20. Resch-Genger, U., Grabolle, M., Cavaliere-Jaricot, S., Nitschke, R. & Nann, T. Quantum dots versus organic dyes as fluorescent labels. *Nat. Methods* **5**, 763–775

(2008).
21. Xu, C., Zipfel, W., Shear, J. B., Williams, R. M. & Webb, W. W. Multiphoton fluorescence excitation: New spectral windows for biological nonlinear microscopy. *Proc. Natl. Acad. Sci. U. S. A.* **93**, 10763–10768 (1996).
22. Efros, A. L. & Nesbitt, D. J. Origin and control of blinking in quantum dots. *Nat. Nanotechnol.* **11**, 661–671 (2016).
23. Hutter, E. & Maysinger, D. Gold nanoparticles and quantum dots for bioimaging. *Microsc. Res. Tech.* **74**, 592–604 (2011).
24. Van den Broek, B., Oosterkamp, T. H. & van Noort, J. A Multifocal Two-Photon Microscopy Setup for Parallel 3D Tracking of Gold Nanorods. *Biophys. J.* **98**, 178a (2010).
25. Zijlstra, P., Paulo, P. M. R. & Orrit, M. Optical detection of single non-absorbing molecules using the surface plasmon resonance of a gold nanorod. *Nat. Nanotechnol.* **7**, 379–382 (2012).
26. Dixit, R. & Cyr, R. Cell damage and reactive oxygen species production induced by fluorescence microscopy: Effect on mitosis and guidelines for non-invasive fluorescence microscopy. *Plant J.* **36**, 280–290 (2003).
27. Knight, M. M., Roberts, S. R., Lee, D. A. & Bader, D. L. Live cell imaging using confocal microscopy induces intracellular calcium transients and cell death. *Am. J. Physiol. - Cell Physiol.* **284**, 1083–1089 (2003).
28. Icha, J., Weber, M., Waters, J. C. & Norden, C. Phototoxicity in live fluorescence microscopy, and how to avoid it. *BioEssays* **39**, 1–15 (2017).
29. Magidson, V. & Khodjakov, A. Circumventing photodamage in live-cell microscopy. *Methods Cell Biol.* **114**, 545–560 (2013).
30. Knobel, K. M., Jorgensen, E. M. & Bastiani, M. J. Growth cones stall and collapse during axon outgrowth in Caenorhabditis elegans. *Development* **126**, 4489–4498 (1999).
31. Maravall, M., Mainen, Z. F., Sabatini, B. L. & Svoboda, K. Estimating intracellular calcium concentrations and buffering without wavelength ratioing. *Biophys. J.* **78**, 2655–2667 (2000).
32. Roechlecke, C., Schaller, A., Knels, L. & Funk, R. H. W. The influence of sublethal blue light exposure on human RPE cells. *Mol. Vis.* **15**, 1929–1938 (2009).
33. Laissue, P. P., Alghamdi, R. A., Tomancak, P., Reynaud, E. G. & Shroff, H. Assessing phototoxicity in live fluorescence imaging. *Nat. Methods* **14**, 657–661 (2017).
34. Schneckenburger, H. *et al.* Light exposure and cell viability in fluorescence microscopy. *J. Microsc.* **245**, 311–318 (2012).
35. Spikes, J. Photosensitization in Mammalian Cells. in *Photoimmunology* 23–49 (Springer US, 1983).
36. Wagner, M. *et al.* Light dose is a limiting factor to maintain cell viability in fluorescence microscopy and single molecule detection. *Int. J. Mol. Sci.* **11**, 956–966 (2010).
37. Liu, X. *et al.* A genetically encoded photosensitizer protein facilitates the rational design of a miniature photocatalytic CO 2 -reducing enzyme. *Nat. Chem.* **10**, 1201–1206 (2018).
38. Bar-Ilan, O. *et al.* Titanium dioxide nanoparticles produce phototoxicity in the developing zebrafish. *Nanotoxicology* **6**, 670–679 (2012).
39. Bianchi, J. I., Stockert, J. C., Buzz, L. I., Blázquez-Castro, A. & Hernán Simonetta, S.

Reliable screening of dye phototoxicity by using a Caenorhabditis elegans fast bioassay. *PLoS One* **10**, 1–15 (2015).
40. Tinevez, J. Y. *et al. A quantitative method for measuring phototoxicity of a live cell imaging microscope*. *Methods in Enzymology* **506**, (Elsevier Inc., 2012).
41. Stockley, J. H. *et al.* Surpassing light-induced cell damage in vitro with novel cell culture media. *Sci. Rep.* **7**, 1–11 (2017).
42. Waldchen, S., Lehmann, J., Klein, T., Van De Linde, S. & Sauer, M. Light-induced cell damage in live-cell super-resolution microscopy. *Sci. Rep.* **5**, 1–12 (2015).
43. Bogdanov, A. M., Kudryavtseva, E. I. & Lukyanov, K. A. Anti-Fading Media for Live Cell GFP Imaging. *PLoS One* **7**, 1–4 (2012).
44. Nishigaki, T., Wood, C. D., Shiba, K., Baba, S. A. & Darszon, A. Stroboscopic illumination usine light-emitting diodes reduces phototoxicity in fluorescence cell imaging. *Biotechniques* **41**, 191–197 (2006).
45. Penjweini, R., Loew, H. G., Hamblin, M. R. & Kratky, K. W. Long-term monitoring of live cell proliferation in presence of PVP-Hypericin: A new strategy using ms pulses of LED and the fluorescent dye CFSE. *J. Microsc.* **245**, 100–108 (2012).
46. Mattheyses, A. L., Simon, S. M. & Rappoport, J. Z. Imaging with total internal reflection fluorescence microscopy for the cell biologist. *J. Cell Sci.* **123**, 3621–3628 (2010).
47. Denk, W., Strickler, J. H. & Webb, W. W. Two-Photon Laser Scanning Fluorescence Microscopy. *Sci. New Ser.* **248**, 73–76 (1990).
48. Chen, B.-C. *et al.* Lattice light-sheet microscopy: Imaging molecules to embryos at high spatiotemporal resolution. *Science (80-.).* **346**, 1257998 (2014).
49. Masters, B. R. *et al.* Mitigating thermal mechanical damage potential during two-photon dermal imaging. *J. Biomed. Opt.* **9**, 1265 (2004).
50. Bixler, J. *et al.* Assessment of tissue heating undertunable near-infrared radiation. *J. Biomed. Opt.* 22.1-22.37 (2009). doi:10.1117/1.JBO.19.7
51. Rockhold, S. A., Quinn, R. D., Wagenen, R. A. V. A. N., Andrade, J. D. & Reichert, M. Total Internal Reflection Fluorescence (TIRF) as a quantitative probe of protein absorption. **150**, 261–275 (1983).
52. Tokunaga, M., Imamoto, N. & Sakata-sogawa, K. Highly inclined thin illumination enables clear single-molecule imaging in cells. *Nature* **5**, 159–161 (2008).
53. Gustafsson, M. G. L. Surpassing the lateral resolution limit by a factor of two using structured illumination microscopy. *J. Microsc.* **198**, 82–87 (2000).
54. Shao, L., Kner, P., Rego, E. H. & Gustafsson, M. G. L. Super-resolution 3D microscopy of live whole cells using structured illumination. *Nat. Methods* **8**, 1044–1048 (2011).
55. Benninger, R. K. P. & Piston, D. W. Two-Photon Excitation Microscopy for the Study of Living Cellsand Tissues. *Curr. Protoc. cell Biol.* **June**, 1–36 (2014).
56. Soeller, C. & Cannell, M. B. Two-Photon Microscopy : Imaging in Scattering Samples and Three-Dimensionally Resolved Flash Photolysis. *Microsc. Res. Tech.* **195**, 182–195 (1999).
57. So, P. T. C., Dong, C. Y., Masters, B. R. & Berland, K. M. Two-Photon Excitation Fluorescence Microscopy. *Annu. Rev. Biomed. Eng.* 399–429 (2000).
58. Chirico, G., Cannone, F., Baldini, G. & Diaspro, A. Two-Photon Thermal Bleaching of Single Fluorescent Molecules. *Biophys. J.* **84**, 588–598 (2003).
59. Bewersdorf, J. & Hell, S. W. Picosecond pulsed two-photon imaging with repetition

rates of 200 and 400 MHz. *J. Microsc.* **191**, 28–38 (1998).
60. Hell, S. W. *et al.* Two-photon near- and far-field fluorescence microscopy with continuous-wave excitation. *Opt. Lett.* **23**, 1238 (1998).
61. Stosiek, C., Garaschuk, O., Holthoff, K. & Konnerth, A. In vivo two-photon calcium imaging of neuronal networks. *Proc. Natl. Acad. Sci. U. S. A.* **100**, 7319–7324 (2003).
62. Schwille, P., Haupts, U., Maiti, S. & Webb, W. W. Molecular dynamics in living cells observed by fluorescence correlation spectroscopy with one- and two-photon excitation. *Biophys. J.* **77**, 2251–2265 (1999).
63. Cole, R. W., Jinadasa, T. & Brown, C. M. Measuring and interpreting point spread functions to determine confocal microscope resolution and ensure quality control. *Nat. Protoc.* **6**, 1929–1941 (2011).
64. Sheppard, C. Image formation in two-photon fluorescence microcopy. *Optik (Stuttg).* 1–4 (1990).
65. Zipfel, W. R., Williams, R. M. & Webb, W. W. Nonlinear magic: Multiphoton microscopy in the biosciences. *Nat. Biotechnol.* **21**, 1369–1377 (2003).
66. Wang, T., Halaney, D., Ho, D., Feldman, M. D. & Milner, T. E. Two-photon luminescence properties of gold nanorods. *Biomed. Opt. Express* **4**, 584–95 (2013).
67. Larson, D. R. *et al.* Water-soluble quantum dots for multiphoton fluorescence imaging in vivo. *Science (80-.).* **300**, 1434–1436 (2003).
68. Gu, M., Gan, X., Kisteman, A. & Xu, M. G. Comparison of penetration depth between two-photon excitation and single-photon excitation in imaging through turbid tissue media. *Appl. Phys. Lett.* **77**, 1551–1553 (2000).
69. Dittrich, P. S. & Schwille, P. Photobleaching and stabilization of fluorophores used for single-molecule analysis with one- and two-photon excitation. *Appl. Phys. B Lasers Opt.* **73**, 829–837 (2001).
70. Eggeling, C., Volkmer, A. & Seidel, C. A. M. Molecular photobleaching kinetics of Rhodamine 6G by one- and two-photon induced confocal fluorescence microscopy. *ChemPhysChem* **6**, 791–804 (2005).
71. Chen, T.-S., Zeng, S.-Q., Luo, Q.-M., Zhang, Z.-H. & Zhou, W. High-Order Photobleaching of Green Fluorescent Protein inside Live Cells in Two-Photon Excitation Microscopy. *Biochem. Biophys. Res. Commun.* **291**, 1272–1275 (2002).
72. Sanchez, E. J., Novotny, L., Holtom, G. R. & Xie, X. S. Room-temperature fluorescence imaging and spectroscopy of single molecules by two-photon excitation. *J. Phys. Chem. A* **101**, 7019–7023 (1997).
73. Patterson, G. H. & Piston, D. W. Photobleaching in Two-Photon Excitation Microscopy. *Biophys. J.* **78**, 2159–2162 (2000).
74. Xi, P., Andegeko, Y., Weisel, L. R., Lozovoy, V. V. & Dantus, M. Greater signal, increased depth, and less photobleaching in two-photon microscopy with 10 fs pulses. *Opt. Commun.* **281**, 1841–1849 (2008).
75. Graham, D. J. L., Tseng, S., Chen, J. H. D. J. & Alexandrakis, G. Dependence of Two-Photon eGFP Bleaching on Femtosecond Pulse Spectral Amplitude and Phase. *J. Fluoresc.* 1775–1785 (2015). doi:10.1007/s10895-015-1667-1
76. Niu, F. *et al.* Photobleaching of ultrashort pulses with different repetition rates in two-photon excitation microscopy. *Laser Phys.* **29**, 046001 (2019).
77. Truong, T. V, Supatto, W., Koos, D. S., Choi, J. M. & Fraser, S. E. Deep and fast live imaging with two-photon scanned light-sheet microscopy. *Nat. Methods 2011 89* **8**, 757

(2011).
78. Drobizhev, M., Makarov, N. S., Tillo, S. E., Hughes, T. E. & Rebane, A. Two-photon absorption properties of fluorescent proteins. *Nat. Methods* **8**, 393–399 (2011).
79. Bewersdorf, J., Pick, R. & Hell, S. W. Multifocal multiphoton microscopy. *Opt. Lett.* **23**, 655 (1998).
80. Fittinghoff, D. N., Wiseman, P. W. & Squier, J. A. Widefield multiphoton and temporally decorrelated multifocal multiphoton microscopy. *Opt. Express* **7**, 273 (2000).
81. Matsumoto, N. *et al.* An adaptive approach for uniform scanning in multifocal multiphoton microscopy with a spatial light modulator. *Opt. Express* **22**, 633 (2014).
82. Poland, S. P. *et al.* Time-resolved multifocal multiphoton microscope for high speed FRET imaging in vivo. *Opt. Lett.* **39**, 6013 (2014).
83. Pozzi, P. *et al.* High-throughput spatial light modulation two-photon microscopy for fast functional imaging. *Neurophotonics* **2**, 015005 (2015).
84. Huisken, J., Swoger, J., Bene, F. Del, Wittbrodt, J. & Stelzer, E. H. K. Optical Sectioning Deep Inside Live Embryos by Selective Plane Illumination Microscopy.
85. Palero, J., Santos, S. I. C. O., Artigas, D. & Loza-Alvarez, P. A simple scanless two-photon fluorescence microscope using selective plane illumination. *Opt. Express* **18**, 8491 (2010).
86. Maruyama, A. *et al.* Wide field intravital imaging by two-photon- excitation digital-scanned light-sheet microscopy (2p-DSLM) with a high-pulse energy laser. *C)* **5**, (2014).
87. Zong, W. *et al.* Large-field high-resolution two-photon digital scanned light-sheet microscopy. *Cell Res.* **25**, 254–257 (2015).
88. Lavagnino, Z., Cella Zanacchi, F., Ronzitti, E. & Diaspro, A. Two-photon excitation selective plane illumination microscopy (2PE-SPIM) of highly scattering samples: characterization and application. *Opt. Express* **21**, 5998 (2013).
89. Zhao, M. *et al.* Cellular imaging of deep organ using two-photon Bessel light-sheet nonlinear structured illumination microscopy. *Biomed. Opt. Express* **5**, 1296 (2014).
90. Hedde, P. N. & Gratton, E. Selective Plane Illumination Microscopy with a Light Sheet of Uniform Thickness Formed by an Electrically Tunable Lens. *Microsc. Res. Tech.* **176**, 139–148 (2018).
91. Supatto, W., Truong, T. V, Débarre, D. & Beaurepaire, E. Advances in multiphoton microscopy for imaging embryos. *Curr. Opin. Genet. Dev.* **21**, 538–548 (2011).
92. Ji, N., Magee, J. C. & Betzig, E. High-speed, low-photodamage nonlinear imaging using passive pulse splitters. *Nat. Methods* **5**, 197–202 (2008).
93. Girkin, J. M. & Carvalho, M. T. The light-sheet microscopy revolution. *J. Opt.* **20**, (2018).
94. Girstmair, J. *et al.* Light-sheet microscopy for everyone? Experience of building an OpenSPIM to study flatworm development. *BMC Dev. Biol.* **16**, (2016).
95. Ponjavic, A., Ye, Y., Laue, E., Lee, S. F. & Klenerman, D. Sensitive light-sheet microscopy in multiwell plates using an AFM cantilever. *Biomed. Opt. Express* **9**, 5863 (2018).
96. McGorty, R. *et al.* Open-top selective plane illumination microscope for conventionally mounted specimens. *Opt. Express* **23**, 16142–53 (2015).
97. Meddens, M. B. M. *et al.* Single objective light-sheet microscopy for high-speed whole-

cell 3D super-resolution. *Biomed. Opt. Express* **7**, 2219 (2016).
98. Mahou, P., Vermot, J., Beaurepaire, E. & Supatto, W. Multicolor two-photon light-sheet microscopy. *Nat. Methods* **11**, 600–601 (2014).
99. Kim, K. H. *et al.* Multifocal multiphoton microscopy based on multianode photomultiplier tubes. *Opt. Express* **15**, 11658 (2007).
100. Martini, J., Andresen, V. & Anselmetti, D. Scattering suppression and confocal detection in multifocal multiphoton microscopy. *J. Biomed. Opt.* **12**, 034010 (2007).
101. Rakotoson, I. *et al.* Fast 3-D Imaging of Brain Organoids With a New Single-Objective Planar-Illumination Two-Photon Microscope. *Front. Neuroanat.* **13**, 1–14 (2019).
102. Quicke, P. *et al.* High speed functional imaging with source localized multifocal two-photon microscopy. *Biomed. Opt. Express* **9**, 3678 (2018).
103. Ingaramo, M. *et al.* Two-photon excitation improves multifocal structured illumination microscopy in thick scattering tissue. *Proc. Natl. Acad. Sci.* **111**, 5254–5259 (2014).